



Biophysical quantification of reorganization dynamics of human pancreatic islets during co-culture with adipose-derived stem cells

Journal:	<i>Analyst</i>
Manuscript ID	AN-ART-02-2022-000222.R1
Article Type:	Paper
Date Submitted by the Author:	06-May-2022
Complete List of Authors:	Torres-Castro, Karina; University of Virginia, Electrical and Computer Engineering Azimi, Mohammad; Tulane University, Department of Biomedical Engineering Varhue, Walter; University of Virginia, Electrical and Computer Engineering Honrado, Carlos; University of Virginia, Electrical and Computer Engineering Peirce, Shayn; University of Virginia, Biomedical Engineering Swami, Nathan; University of Virginia, Electrical and Computer Engineering



Journal Name

ARTICLE

Biophysical quantification of reorganization dynamics of human pancreatic islets during co-culture with adipose-derived stem cells

Received 00th January 20xx,
Accepted 00th January 20xx

DOI: 10.1039/x0xx00000x
www.rsc.org/

Karina Torres-Castro^a, Mohammad S. Azimi^b, Walter B. Varhue^a, Carlos Honrado^a, Shayn M. Peirce^b and Nathan S. Swami^{*, a}

Islet transplantation is a potential therapy for type 1 diabetes, but it is expensive due to limited pancreas donor numbers and the variability in islet quality. The latter is often addressed by co-culture of harvested islets with stem cells to promote *in vitro* remodeling of their basement membrane and enable expression of angiogenic factors for enhancing vascularization. However, given the heterogeneity in islet size, shape and function, there is a need for metrics to assess the reorganization dynamics of single islets over the co-culture period. Based on shape-evolution of individual multi-cell aggregates formed during co-culture of human islets with adipose derived stem cells and the pressures required for their bypass through microfluidic constrictions, we present size-normalized biomechanical metrics for monitoring the reorganization. Aggregates below a threshold size exhibit faster reorganization, as evident from rise in their biomechanical opacity and tightening of their size distribution, but this size threshold increases over culture time to include a greater proportion of the aggregates. Such biomechanical metrics can quantify the subpopulation of reorganized aggregates by distinguishing them versus those with incomplete reorganization, over various timepoints during the co-culture.

Introduction

T1 diabetes (T1D) is a debilitating autoimmune disease that is currently treated by insulin therapies, but these do not offer the fine control needed for regulating the endocrine response and they neglect the multiple functions served by the pancreas. Transplantation of human islets of Langerhans (h-islets) is emerging as a potential therapy¹⁻³. However, limitations in donor numbers and variability in quality of islets have led to poor engraftment outcomes, including inadequate revascularization^{4,5} and adverse immune responses^{6,7} that increase transplant costs. Improved *in vitro* processing to increase the number of functional islets can promote their vascularization and insulin secretion outcomes *in vivo*⁸.

The co-transplantation of harvested islets with stem cells⁹ or their *in vitro* co-culture prior to transplantation^{10,11} is being explored to promote re-growth of the islet basement membrane and enable expression of angiogenic factors to enhance vascularization¹², for improving the functional quality and reducing the variability of the graft. Specifically, islet co-

transplantation with mesenchymal stem cells¹³ and adipose derived stem cells (ADSCs)¹⁴ promotes islet survival and insulin function of the graft in mice, while reducing the number of islets needed for diabetes reversal, by making the islets more likely to remain viable and vascularize *in vivo* after transplantation^{15,16}. Such methods would also reduce the need to harvest islets from multiple organ donors, thereby reducing immune rejection. However, there are no metrics for monitoring the biophysical reorganization on a single-islet basis, which is required due to heterogeneity in islet size, shape and functional outcomes¹⁷. Such metrics would allow for rapid identification and separation of functional islets, thereby standardizing assessment of their quality and enabling scale-up of transplant numbers.

Following harvest from the donor pancreas, islets are placed in culture media to allow for morphology change¹⁸. This is characterized by gradual recovery of their rigidity over several days due to *in vitro* remodeling of their basement membrane¹⁹⁻²¹ that promotes their vascularization ability after transplantation²². The associated alterations in biomechanical properties of islets correlate with their vascularization potential²³, insulin expression²⁴ and inflammatory responses²⁵, post-transplantation. Microfluidic techniques²⁶ with feature sizes in the range of single cells and multi-cell aggregates, use tangential flows and microscale constrictions to controllably deform biological objects and measure their biomechanical properties. In recent years, several high throughput

^a Department of Electrical & Computer Engineering, University of Virginia, Charlottesville, Virginia-22904, USA.

^b Department of Biomedical Engineering, University of Virginia, Charlottesville, Virginia-22904, USA.

* Corresponding Author. Fax: +1-434-924-8818. Email: nswami@virginia.edu.

† Electronic Supplementary Information (ESI) available: See

DOI: 10.1039/x0xx00000x

microfluidic techniques for measuring deformability differences between individual cells have been developed^{27,28}. Herein, pressure driven flow across constricting structures is used to induce particle deformation, as measured by particle transit time, threshold bypass pressure²⁹, induced hydrodynamic or electrical resistance³⁰, and particle shape alterations under shear flow³¹. However, multi-cell aggregates are spread over a far broader range of size and shape distributions than individual cells, which poses measurement challenges. Furthermore, the high-pressure differentials usually used for deformability-based cell separation can damage multi-cell aggregates³² due to the lower yield strength of their intercellular regions versus that of the component cells³³, highlighting the need for alternate analytical methods.

In this work, we seek to develop metrics to monitor the biophysical reorganization dynamics of the multi-cell h-islet ADSC aggregate during co-culture, by comparing on a single aggregate basis, the biomechanical opacity metric determined by microfluidic deformation (Fig. 1A) versus from microscopic observations (Fig. 1C). While imaging methods suggest the occurrence of reorganization within each aggregate during the co-culture, they are unable to quantify the alterations in absence of 3D visualization abilities and their measurement throughput is not sufficient for dynamic monitoring. Hence, microfluidic deformability measurements to compute biomechanical opacity of single islets can provide a quantitative and high throughput metric, which can be used together with microscopy and endpoint immunoassays (Fig. 1B) of angiogenic and basement membrane factors, to provide multi-modal information on islet basement membrane reorganization dynamics over the co-culture period. Based on bypass pressure measurements on aggregates through microfluidic constrictions (Fig. 1A1-A2), the biomechanical opacity metric can delineate the completion time for subpopulations with remodeled islet basement membrane characteristics during co-culture. This biophysical metric can eventually be used to quantify and separate the fraction of

islets that have reorganized their basement membranes after co-culture with stem cells.

Experimental Methods

Human Pancreatic Islet Isolation: Pancreas were provided by organ procurement organizations with research consent from donors. For isolation of pancreatic islets^{34,35}, the pancreas was injected with collagenase (Roche Liberase HI; Roche: Indianapolis, IN) and then digested in a Ricordi chamber with a close-loop circulation system. The pancreatic tissue digestion and islet dissociation were conducted at 35–37°C. Islets were purified using UIC-UW/Biocoll (UIC-UB) continuous density gradient in a COBE 2991 Cell Separator (Terumo BCT; Lakewood, CO)³⁶. Isolated human islets were then cultured in CMRL 1066 medium with 5% human albumin (Corning; Corning, NY) at 37°C for 24 hrs.

Co-culture of human islets with ADSCs: Adipose-derived stem cells (ADSCs) were expanded at ~5000 cells/cm² (Corning; Corning, NY) using Rooster Nourish-MSC medium (RoosterBio; Frederick, MD) until they reached 70% confluency. Cells from passage numbers 3-5 were dissociated and lifted using Accutase (ThermoFisher; Waltham, MA) and used for the experiment. Human pancreatic islets were placed individually in 50 μ L human islet medium (CMRL 1066 without phenol red, L-glutamine; Corning; Corning, NY) in ultra-low attachment round bottom 96-well plates (Corning; Corning, NY). ADSCs were suspended in human islet medium at 20k/ml density, and 200 μ L of the ADSC suspension was added to each well. ADSCs gradually attached to the outer surface of the islets, and the co-cultures were maintained under standard incubator conditions (5% CO₂, 37°C). At different time points over six days (24, 48, 72, 96, 120, and 144 hours), the islets and attached ADSCs were collected for analysis. Control cultures of islets in the absence of ADSCs, as well as ADSCs in the absence of islets were also maintained under the same culture conditions for the duration of the experiment.

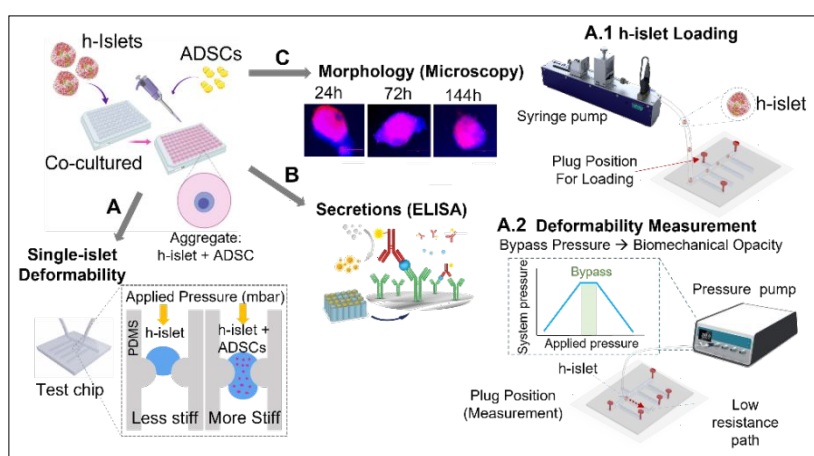


Figure 1. Aggregates of h-islets co-cultured with ADSCs are analysed by: A. Single islet deformability on microfluidic chip. B. Secretions of angiogenic and basement membrane factors by ELISA. C. Fluorescence microscopy to image morphology alterations over culture time. Overview of deformability measurement: A.1: h-islets are loaded in the chip. A.2: Bypass pressure measurement through 80 μ m constriction.

Journal Name

ARTICLE

Fluorescence microscopy of h-islet aggregates: Fluorescence images of single aggregates of h-islets after co-culture with ADSCs in well plates were measured using a EVOS FL cell imaging microscope (ThermoFisher Scientific), under a magnification of 20x, using Dil (1,1'-Dioctadecyl- 3,3,3',3'-Tetramethylindocarbocyanine Perchlorate) (Invitrogen), which is lipophilic stain that is specific to ADSCs, and Hoechst 33342 (Bisbenzimidazole) (ThermoFisher) fluorescent stain that is specific to the h-islet membrane.

Basement Membrane and Angiogenesis Analysis: Conditioned media from co-cultured ADSCs and h-islets was collected for the analysis of basement membrane and angiogenic factors after 144 hours to compare versus media from ADSCs cultured without islets and from islets cultured without ADSCs as controls. These factors were quantified using the Proteome Profiler Human Angiogenesis Array Kit (R&D Systems; Minneapolis, MN).

Fabrication of microfluidic device: The microfluidic device (Fig. 1A) was fabricated by photolithography of the master (EVG 620 mask aligner), using a photo mask (PhotoSciences) and a negative photoresist (SU-8 2150, MicroChem) for pattern definition. Micro-molding with PDMS or polydimethylsiloxane (Sylgard 184, Dow Corning) was performed using uncured elastomer base to curing agent in the 5:1 ratio and crosslinking at 60 C for 8h to obtain microchannels of 500 μm depth with 80 μm constrictions. After curing, the PDMS chip was released from the master; the PDMS features were diced, and the inlets and outlets were drilled with a biopsy punch. The chip was bonded to a glass cover slip after oxygen plasma treatment (PDC-001 Harrick Plasma cleaner).

Bypass pressure measurements of single-islets: For bypass pressure measurements (Fig 1.A1-A2), a syringe pump (neMESYS 290N, Cetoni GmbH) was used to load single h-islets into the microfluidic chip and a pressure controller (Fluigent MFCS-EZ) was used to adjust the applied pressure in the channel to pass h-islet through 80 μm constrictions.

Imaging of h-islets for shape and area quantification: A series of videos were taken on each measured h-islet before, during and after passage through the microfluidic constriction, using a CMOS Orca-Flash 4.LT digital camera (Hamamatsu) coupled with a Carl Zeiss inverted microscope (Axio Observer Z.1). The islets were also imaged by fluorescence microscopy to ensure maintenance of viability. Image processing to determine the h-islet particle area measurements were done using the Fiji software from the National Institute of Health (NIH).

Data processing and statistical analysis: One-way ANOVA with Tukey's multiple comparison tests and t-tests with Welch's correction were applied to compare differences between time points and on unpaired samples using GraphPad Prism. A custom-made MATLAB (R2017a) script was used to perform a principal component analysis (PCA) for calculating the 95% confidence ellipses from the obtained data. The covariance matrix was calculated to extract the eigenvectors (principal components)³⁷ to plot the h-islet area versus bypass pressure under control and ADSC co-culture conditions into confidence ellipses. The largest spread of the data (first principal component) corresponds to the major axis, and the minor axis is the perpendicular component (second principal component) with the second highest variance³⁸. The bypass pressure was normalized based on area of the aggregate to compute biomechanical opacity values that were used to visualize the deformability response trends of the h-islets co-cultured with ADSC, in comparison with h-islet controls.

Results and discussion

Shape-based monitoring of aggregate reorganization:

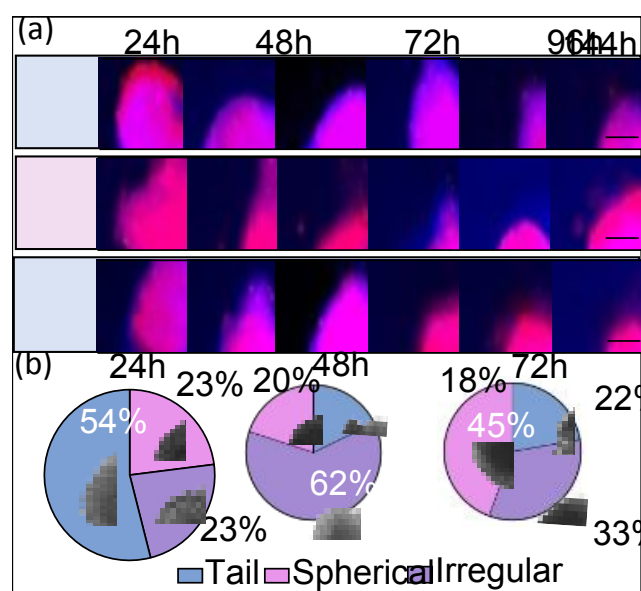


Figure 2: Integration and reorganization of h-islets after co-culture with ADSCs. (a) Representative fluorescence images over 6 days of co-culture; (b) Brightfield images to quantify shape distributions of 42 islets per culture condition.

The reorganization dynamics of single h-islet aggregates (h-islet plus ADSCs) was monitored over the co-culture period by

fluorescence imaging to assess the integration of ADSCs (pink) with the h-islets (purple), as well as by bright field imaging to follow the shape alterations. From the representative fluorescence images (Fig. 2a), while ADSC regions merge with the islet tissue, right from the 24 h data point, the shape evolution towards a spherical morphology occurs more gradually over the 6-day co-culture period. Based on bright field images of 42 multicell aggregates at each timepoint (24 h, 48 h and 72 h), the co-cultured h-islet plus ADSC aggregates were classified to determine proportions within three distinct morphologies: spherical, tail, and irregular shapes (Fig. 2b). While a majority of the co-cultured aggregates exhibit tail morphologies at the 24 h time point, the predominant morphology at the 48 h timepoint is irregular and the aggregates become spherical onwards from the 72 h timepoint. The shape reorganization from imaging does not show a dependence on aggregate size (rows of Fig. 2a). Since merging of the ADSC and islet tissue is apparent right from the 24 h co-culture timepoint (Fig. 2a), we use the total area of the multi-cell aggregate for all subsequent normalization within biomechanical studies on co-cultured h-islets.

Biomechanical opacity indicates size-dependence in h-islet reorganization: The biomechanical alterations of h-islets due to basement membrane remodeling during co-culture with ADSCs were quantified based on the bypass pressure level for passage of individual aggregates (h-islet integrated with ADSCs) through 80 μm constrictions (Fig. 1 A1-A2). The plots of bypass pressure for each aggregate versus its measured area (from bright field images) are in Fig. 3a (24 h co-culture) and Fig. 3b (72 h co-culture). Respective plots are also shown for the control h-islets that were maintained without ADSCs in the same media for the timepoints. The plots include confidence ellipses for the cases of 1σ and 2σ in data spread (σ is standard deviation). Based on this, while the spread in data for “control” islets is not altered after 24 h of co-culture with ADSCs, this spread is significantly lowered after 72 h of co-culture with ADSCs, likely since aggregate reorganization over this co-culture period leads to tightening of their size and

stiffness property distributions. Hence, a greater proportion of the aggregates has likely reorganized at the 72 h versus the 24 h co-culture timepoint. However, as elaborated below, slope of the data points on the bypass pressure versus aggregate area plot (major axis of the ellipse) suggests a degree of heterogeneity in reorganization time for each aggregate type. Hence, we seek to assess the phenotype that can be used to measure the reorganization dynamics of each aggregate. The bypass pressure level for “control” h-islets increases with their area (i.e., positive slope), as expected from volumetric scaling of flow around the aggregate exterior. The trend is similar for h-islet aggregates after ADSC co-culture at the 24 h timepoint, with only a minor slope reduction. However, the bypass pressure becomes invariant with aggregate area at the 72 h timepoint, as apparent from the near-zero slope. A size-dependence in the h-islet reorganization dynamics during its co-culture with ADSCs can explain this slope alteration. If the h-islet aggregates below a threshold size reorganize more effectively over the 72 h co-culture period versus those above a threshold size level, and assuming completion of reorganization leads to higher biomechanical stiffness, then the bypass pressure values would be enhanced for the smaller-sized subpopulation versus the larger-sized subpopulation to cause the observed slope alteration. This size-based heterogeneity in reorganization is not observed for control h-islets or for the 24-h co-cultured h-islet aggregates that have undergone only minimal reorganization, since they exhibit a steady rise in bypass pressure with aggregate area. However, size-based heterogeneity in reorganization likely sets in at the 48 h (ESI: Fig. S1b) and 72 h timepoints, due to a subpopulation that has reorganized and another that has not reorganized. The caveat is that there may be size alterations of h-islet aggregates during the reorganization over the co-culture period, which would also alter their bypass pressure. Hence, an ANOVA test was performed to correlate the bypass pressure with the size distribution of the h-islet aggregate, so that we can identify the relationship between the variables (aggregate area and bypass pressure).

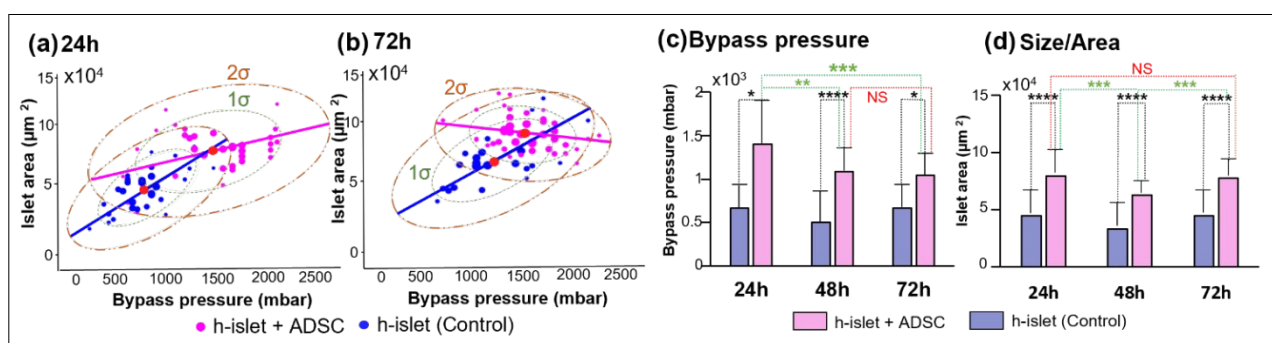


Figure 3: Bypass pressure of individual co-cultured h-islet + ADSC aggregates and h-islet controls plotted as h-islet area (μm^2) vs bypass pressure (mbar) after: (a) 24 h, and (b) 48 h co-culture (controls in blue and h-islets + ADSC aggregates in pink). The plot at 48 h is in supplementary material (Fig. S1b). One-way ANOVA showing 1σ (inner error ellipse) and 2σ (outer error ellipse) for: (c) bypass pressure and, (d) h-islet area, presented as mean SD with 95% CI, followed by a Tukey's multiple comparison test with ****p-value<0.0001, ***p-value<0.001, **p-value<0.01, *p-value<0.05 and NS is not significant. A two tailed t-test with Welch's correction (unpaired samples) was also done for comparing controls with their corresponding h-islets + ADSC for each time point.

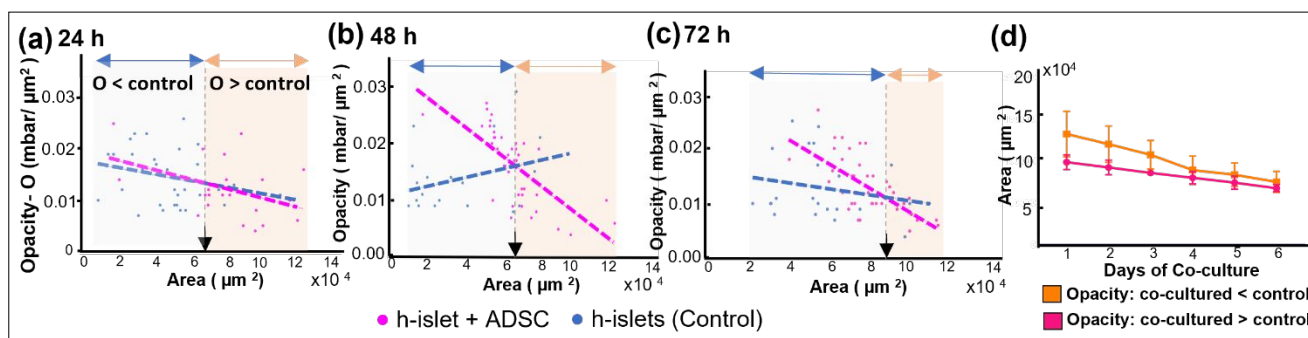


Figure 4: Area-normalized bypass pressure expressed as biomechanical opacity ($\text{mbar}/\mu\text{m}^2$) plotted in log-scale versus measured area for the h-islet aggregate after ADSC co-culture versus the control (no ADSC in co-culture) after: (a) 24 h, (b) 48 h and (c) 72 h of co-culture show two distinct sized subpopulations (vertical dash line): one of smaller area with biomechanical opacity higher than the control and another of larger area with lower biomechanical opacity lower than the control. (d) Size evolution for these subpopulations of co-cultured aggregates shows that the size differences become progressively smaller over the co-culture period (Day 1 to Day 6), presumably due to the reorganization leading to stiffer islets of smaller area, as suggested by the tighter data spread in Fig. 3a vs. Fig. 3b.

The statistical significance plots over the co-culture time for bypass pressure (Fig. 3c) and area of the aggregates (Fig. 3d) show that a consideration based solely on exterior size changes over the 24 h to 72 h ADSC co-culture period is not sufficient to explain the large bypass pressure alterations that were observed. For instance, while the bypass pressure alterations between co-cultured aggregates at the 24 h versus 72 h periods show a high degree of statistical significance (green stars in Fig. 3c), size alterations for the respective samples show a lower degree of statistical significance (“not significant” or NS in Fig. 3d). To further characterize the interplay of aggregate size and inherent stiffness alterations during h-islet reorganization under ADSC co-culture, on the measured bypass pressure, we computed biomechanical opacity (O) as a size-normalized index, using the average aggregate area at each time point of the sample as the reference for normalization of the bypass pressure values. Hence, the biomechanical opacity versus area plot of Fig. 4a–4c for co-cultured h-islet aggregates should show near-zero slope. In fact, this is the case for slope of control h-islets after 24 h, 48 h and 72 h with no ADSC co-culture, as well as for islets co-cultured with the ADSCs for 24 h, wherein there is minimal difference in opacity for the control versus co-cultured h-islet populations (Fig. 4a). On the other hand, opacity of the co-cultured h-islet aggregates starts to exhibit a size-dependent divergence versus that observed for control h-islets, after the 48 h (Fig. 4b) and 72 h co-culture timepoints (Fig. 4c). Based on this, we delineate the aggregate size at which the divergence in opacity begins to occur for the co-cultured h-islets versus the control islets. The aggregate size threshold for opacity divergence is seen to progressively increase from the 24 h (Fig. 4a) to 48 h (Fig. 4b) to 72 h (Fig. 4c) co-culture

timepoints, per aggregate areas (μm^2 units) of: 6.3×10^4 (Fig. 4a), 6.5×10^4 (Fig. 4b) and 8.3×10^4 (Fig. 4c). Hence, reorganization of the co-cultured h-islet aggregates occurs within 48 h for the smaller islets (those with area $< 6.5 \times 10^4 \mu\text{m}^2$ per Fig. 4b) to reach inherent biomechanical stiffness levels (as measured by opacity) that are greater than those of the control islets, but the larger islets (those with area $> 6.5 \times 10^4 \mu\text{m}^2$) continue to exhibit lower biomechanical stiffness (based on opacity). Similarly, islet aggregate reorganization after 72 h of co-culture is apparent for the population up to a higher size level, i.e., those with an area of $8.3 \times 10^4 \mu\text{m}^2$ (Fig. 4c). In fact, in comparison to control h-islets, the co-cultured h-islet aggregates with higher biomechanical opacity are always the subpopulation with smaller than threshold size level, and the co-cultured h-islet aggregates showing lower biomechanical stiffness versus control h-islets are always the subpopulation with the larger than threshold size. A comparison of the size distribution of these two subpopulations is shown in Fig. 4d at each of the co-culture time points (Day 1 – Day 6). This indicates that while two distinct size-based subpopulations are apparent for the co-cultured aggregates at the 24 h (Day 1), 48 h (Day 2) and 72 h (Day 3) timepoints, the respective subpopulations overlap in size distributions onward from Day 4 to Day 6. Also, due to reorganization of the co-cultured h-islet aggregates, their net size becomes progressively lowered over the entire culture period (Day 1 – Day 6 in Fig. 4d). Since smaller-sized aggregates reorganize more rapidly, the progressively lowered aggregate size likely speeds up the reorganization process, thereby tightening their size and stiffness property distributions, as observed in Fig. 3a vs. 3b, due to onset of

basement membrane remodeling. This distinct biomechanical opacity profile can identify reorganized h-islets.

Co-culture enhances secretion of pro-angiogenic and basement membrane-altering factors: After 144 hours (6 days) in culture, h-islets cultured with ADSCs secreted higher levels of pro-angiogenic factors including PDGF, PLGF, FGF-2, and VEGF (Fig. 5a) and basement membrane altering factors including MMPs and TIMPs (Fig. 5b) in the conditioned media than was secreted by human islets cultured alone (i.e., in the absence of ADSCs) or by ADSCs cultured alone. For example, VEGF secretion by human islets co-cultured with ADSCs was nearly 8-fold higher than VEGF secretion by islets cultured alone. The 5-fold higher level of VEGF secretion by ADSCs versus the respective level from islets cultured alone suggests that co-culture of islets with ADSCs boosts VEGF secretion levels by both islets and ADSCs in a synergistic manner. Other functional assays on co-cultured versus control h-islets, such as static GSIS (glucose stimulated insulin release) and dynamic measurements of intracellular calcium and insulin secretion³⁹, are challenging to perform at single-islet sensitivity. The lack of methods to normalize functional assays for islet heterogeneity made it difficult to compare versus the biomechanical opacity index that is size-normalized and performed at single-islet sensitivity. Such functional assays at single-islet sensitivity need to be examined in future work.

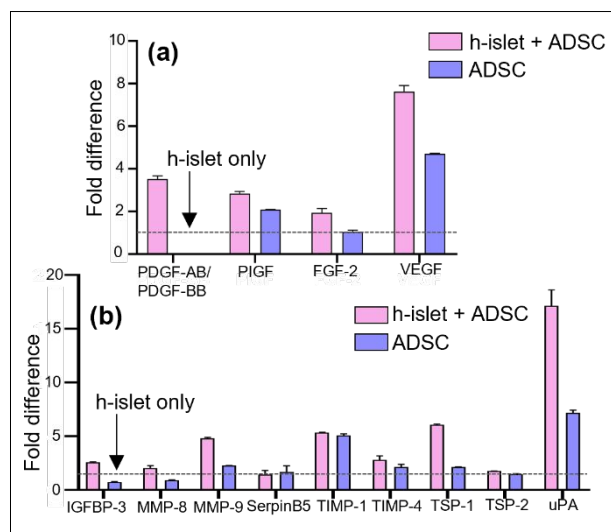


Figure 5. Profiling of conditioned media with ELISA shows that co-culture of human islets with ADSCs (pink bars) for six days (144 hours) increases secretion of matrix modifying proteins versus the respective levels from ADSCs cultured in isolation (blue bars) relative to islets cultured alone (dashed line). Error bars from multiple runs shown as mean \pm σ .

Conclusions

The reorganization process of h-islet aggregates during their co-culture with ADSCs, which leads to enhanced expression of angiogenic and basement membrane altering factors, was characterized over time on a single-aggregate basis, using imaging and microfluidic biomechanical measurements. Based

on fluorescence and bright field images, it is apparent that the co-cultured h-islet aggregates are merged with ADSCs, right from the 24 h co-culture timepoint, but their shape reorganization occurs more slowly and extends over the 6-day co-culture period. The reorganization process causes the co-cultured h-islet aggregates to transition from those predominantly with tails at the 24 h timepoint, to those with irregular shapes at the 48 h timepoint and to those with spherical shapes onward from the 72 h timepoint. The bypass pressure of single aggregates measured as a function of their area shows that h-islet reorganization over the co-culture period leads to tightening of their size and stiffness property distributions. Furthermore, co-cultured h-islet aggregates below a threshold size level reorganize more effectively to exhibit more substantial increases in biomechanical opacity versus those above a threshold size level that take longer to reorganize and exhibit less proportionate rise in biomechanical opacity. While the threshold size level required for more complete h-islet reorganization starts with the smaller sized subpopulation, this size threshold is upshifted over the culture period to include h-islet aggregates of progressively larger sizes. In fact, h-islets co-cultured with ADSCs show two distinct subpopulations: one of higher biomechanical opacity with smaller than a threshold size, and one of lower biomechanical opacity with larger than a threshold size. However, the threshold for size differences between the two subpopulations becomes progressively closer over the co-culture period. Hence, h-islet reorganization during ADSC co-culture likely causes basement membrane remodeling to lead to stiffer islets of smaller area that exhibit tighter spreads in their bypass pressure versus size plots. Since the subpopulation of h-islets that exhibit faster reorganization can be identified based on their distinct biomechanical opacity, this metric can potentially be applied to quantify and separate the fraction of h-islet aggregates that have reorganized after ADSC co-culture.

Supporting Information

† Supporting Information (SI) on confidence ellipses for size and bypass pressure of aggregates over various co-culture periods (S1) and the associated images (S2) is available.

Author Contributions and Conflicts of Interest

K. Torres-Castro: Methodology, Investigation, Data Curation; M. S. Azimi: Methodology, Investigation, Data Curation; W. B. Varhue: Formal analysis; C. Honrado: Formal analysis; S. M. Peirce: Conceptualization, Resources, Supervision; N. S. Swami: Conceptualization, Methodology, Resources, Writing, Supervision, Project administration, Funding acquisition. Authors have no conflicts of interest to declare.

Acknowledgements

Funding from the Paul Manning Launchpad Award, US AFOSR contract FA2386-21-1-4070, and University of Virginia's Advanced Biomanufacturing and Engineering-in-Medicine initiatives are acknowledged.

References

- Langer, R. In *Islet transplantation: lessons learned since the Edmonton breakthrough*, Transplantation proceedings, Elsevier: 2010; pp 1421-1424.
- Ricordi, C.; Strom, T. B., Clinical islet transplantation: advances and immunological challenges. *Nature reviews. Immunology* **2004**, *4* (4), 259.
- Bottino, R.; Knoll, M. F.; Knoll, C. A.; Bertera, S.; Trucco, M. M., The future of islet transplantation is now. *Frontiers in medicine* **2018**, *5*, 202.
- Heuser, M.; Wolf, B.; Vollmar, B.; Menger, M. D., Exocrine contamination of isolated islets of Langerhans deteriorates the process of revascularization after free transplantation. *Transplantation* **2000**, *69* (5), 756-761.
- Bowers, D.T., Song, W., Wang, L.H., Ma, M., Engineering the vasculature for islet transplantation. *Acta Biomaterialia* **2019**, *95*, pp.131-151.
- Coronel, M.M., Martin, K.E., Hunckler, M.D., Barber, G., O'Neill, E.B., Medina, J.D., Opri, E., McClain, C.A., Batra, L., Weaver, J.D., Lim, H.S., Qiu, P., Botchwey, E.A., Yolcu, E.S., Shirwan, H., Garcia, A.J. Immunotherapy via PD-L1-presenting biomaterials leads to long-term islet graft survival. *Science Advances* **2020**, *6*(35), eaba5573.
- Ichii, H.; Pileggi, A.; Molano, R. D.; Baidal, D. A.; Khan, A.; Kuroda, Y.; Inverardi, L.; Goss, J. A.; Alejandro, R.; Ricordi, C., Rescue purification maximizes the use of human islet preparations for transplantation. *American journal of transplantation* **2005**, *5* (1), 21-30.
- Shapiro, A. J.; Pokrywczynska, M.; Ricordi, C., Clinical pancreatic islet transplantation. *Nature Reviews Endocrinology* **2017**, *13* (5), 268-277.
- Ito, T.; Itakura, S.; Todorov, I.; Rawson, J.; Asari, S.; Shintaku, J.; Nair, I.; Ferreri, K.; Kandeel, F.; Mullen, Y., Mesenchymal stem cell and islet co-transplantation promotes graft revascularization and function. *Transplantation* **2010**, *89* (12), 1438-1445.
- Yu, S. P.; Wei, Z.; Wei, L., Preconditioning strategy in stem cell transplantation therapy. *Translational stroke research* **2013**, *4* (1), 76-88.
- Rackham, C. L.; Dhadda, P. K.; Chagastelles, P. C.; Simpson, S. J. S.; Dattani, A. A.; Bowe, J. E.; Jones, P. M.; King, A. J. F., Pre-culturing islets with mesenchymal stromal cells using a direct contact configuration is beneficial for transplantation outcome in diabetic mice. *Cytotherapy* **2013**, *15* (4), 449-459.
- Kang, S.; Park, H. S.; Jo, A.; Hong, S. H.; Lee, H. N.; Lee, Y. Y.; Park, J. S.; Jung, H. S.; Chung, S. S.; Park, K. S., Endothelial progenitor cell cotransplantation enhances islet engraftment by rapid revascularization. *Diabetes* **2012**, *61* (4), 866-876.
- Hayward, J. A.; Ellis, C. E.; Seeberger, K.; Lee, T.; Salama, B.; Mulet-Sierra, A.; Kuppan, P.; Adesida, A.; Korbitt, G. S., Cotransplantation of mesenchymal stem cells with neonatal porcine islets improve graft function in diabetic mice. *Diabetes* **2017**, *66* (5), 1312-1321.
- Ohmura, Y.; Tanemura, M.; Kawaguchi, N.; Machida, T.; Tanida, T.; Deguchi, T.; Wada, H.; Kobayashi, S.; Marubashi, S.; Eguchi, H., Combined transplantation of pancreatic islets and adipose tissue-derived stem cells enhances the survival and insulin function of islet grafts in diabetic mice. *Transplantation* **2010**, *90* (12), 1366-1373.
- Hematti, P.; Kim, J.; Stein, A. P.; Kaufman, D., Potential role of mesenchymal stromal cells in pancreatic islet transplantation. *Transplantation reviews* **2013**, *27* (1), 21-29.
- Hubber, E. L.; Rackham, C. L.; Jones, P. M., Protecting islet functional viability using mesenchymal stromal cells. *Stem cells translational medicine* **2021**.
- Nourmohammadzadeh, M., Xing, Y., Lee, J.W., Bochenek, M.A., Mendoza-Elias, J.E., McGarrigle, J.J., Marchese, E., Chun-Chieh, Y., Eddington, D.T., Oberholzer, J. and Wang, Y. A microfluidic array for real-time live-cell imaging of human and rodent pancreatic islets. *Lab Chip* **2016**, *16*(8), 1466-1472.
- Kin, T.; Senior, P.; O'Gorman, D.; Richer, B.; Salam, A.; Shapiro, A. M. J., Risk factors for islet loss during culture prior to transplantation. *Transplant International* **2008**, *21* (11), 1029-1035.
- Stendahl, J. C.; Kaufman, D. B.; Stupp, S. I., Extracellular matrix in pancreatic islets: relevance to scaffold design and transplantation. *Cell transplantation* **2009**, *18* (1), 1-12.
- Wang, R. N.; Paraskevas, S.; Rosenberg, L., Characterization of integrin expression in islets isolated from hamster, canine, porcine, and human pancreas. *Journal of Histochemistry & Cytochemistry* **1999**, *47* (4), 499-506.
- Smink, A. M.; de Vos, P., Therapeutic strategies for modulating the extracellular matrix to improve pancreatic islet function and survival after transplantation. *Current diabetes reports* **2018**, *18* (7), 1-7.
- Irving-Rodgers, H.; Choong, F. J.; Hummitzsch, K.; Parish, C.; Rodgers, R.; Simeonovic, C., Pancreatic islet basement membrane loss and remodeling after mouse islet isolation and transplantation: impact for allograft rejection. *Cell transplantation* **2014**, *23* (1), 59-72.
- LaValley, D. J.; Reinhart-King, C. A., Matrix stiffening in the formation of blood vessels. *Advances in Regenerative Biology* **2014**, *1* (1), 25247.
- Nyitray, C. E.; Chavez, M. G.; Desai, T. A., Compliant 3D microenvironment improves β -cell cluster insulin expression through mechanosensing and β -catenin signaling. *Tissue Eng Pt A* **2014**, *20* (13-14), 1888-1895.
- Nagy, N.; de la Zerda, A.; Kaber, G.; Johnson, P. Y.; Hu, K. H.; Kratochvil, M. J.; Yadava, K.; Zhao, W.; Cui, Y.; Navarro, G., Hyaluronan content governs tissue stiffness in pancreatic islet inflammation. *Journal of Biological Chemistry* **2018**, *293* (2), 567-578.
- Luan, Q.; Macaraniag, C.; Zhou, J.; Papautsky, I., Microfluidic systems for hydrodynamic trapping of cells and clusters. *Biomicrofluidics* **2020**, *14* (3), 031502.
- Zheng, Y.; Nguyen, J.; Wei, Y.; Sun, Y., Recent advances in microfluidic techniques for single-cell biophysical characterization. *Lab on a Chip* **2013**, *13* (13), 2464-2483.
- Qi, D.; Hoelzle, D.; Rowat, A., Probing single cells using flow in microfluidic devices. *The European Physical Journal Special Topics* **2012**, *204* (1), 85-101.
- Myrand-Lapierre, M.-E.; Deng, X.; Ang, R. R.; Matthews, K.; Santoso, A. T.; Ma, H., Multiplexed fluidic plunger mechanism for the measurement of red blood cell deformability. *Lab on a Chip* **2015**, *15* (1), 159-167.
- Zheng, Y.; Nguyen, J.; Wang, C.; Sun, Y., Electrical measurement of red blood cell deformability on a microfluidic device. *Lab on a Chip* **2013**, *13* (16), 3275-3283.
- Otto, O.; Rosendahl, P.; Mietke, A.; Golfier, S.; Herold, C.; Klauke, D.; Girardo, S.; Pagliara, S.; Ekpenyong, A.; Jacobi, A., Real-time deformability cytometry: on-the-fly cell mechanical phenotyping. *Nature methods* **2015**, *12* (3), 199-202.
- Varhue, W. B.; Langman, L.; Kelly-Goss, M.; Lataillade, M.; Brayman, K. L.; Pearce-Cottler, S.; Swami, N. S., Deformability-based microfluidic separation of pancreatic islets from exocrine acinar tissue for transplant applications. *Lab on a Chip* **2017**, *17* (21), 3682-3691.
- Baraniak, P. R.; Cooke, M. T.; Saeed, R.; Kinney, M. A.; Fridley, K. M.; McDevitt, T. C., Stiffening of human mesenchymal stem cell spheroid microenvironments induced by incorporation of gelatin microparticles. *Journal of the mechanical behavior of biomedical materials* **2012**, *11*, 63-71.
- Qi M, Barbaro B, Wang S, Wang Y, Hansen M, Oberholzer J. Human Pancreatic Islet Isolation: Part I: Digestion and Collection of Pancreatic Tissue. *J Vis Exp JoVE*. 2009 [cited 4 Nov 2019]. doi:10.3791/1125

ARTICLE

Journal Name

- 1
2
3 35 Qi M, Barbaro B, Wang S, Wang Y, Hansen M, Oberholzer J. Human
4 pancreatic islet isolation: Part II: purification and culture of human
5 islets. *J Vis Exp JoVE*. 2009. doi:10.3791/1343
6 36 Barbaro B, Salehi P, Wang Y, Qi M, Gangemi A, Kuechle J, et al.
7 Improved human pancreatic islet purification with the refined UIC-
8 UB density gradient. *Transplantation*. 2007;84: 1200–1203.
9 doi:10.1097/01.tp.0000287127.00377.6f
10 37 Wold, S.; Esbensen, K.; Gelaldi, P., *Principal Component Analysis*.
11 *Chemometrics and Laboratory Systems* **1987**, 2, 37-52.
12 38 Ringnér, M., What is principal component analysis? *Nat. Biotechnol.*
13 **2008**, 28, 303-304.
14 39 Adewola, A.F., Lee, D., Harvat, T., Mohammed, J., Eddington, D.T.,
15 Oberholzer, J. and Wang, Y.. Microfluidic perfusion and imaging
16 device for multi-parametric islet function assessment. *Biomedical*
17 *microdevices* **2010**, 12(3), 409-417.
18
19
20
21
22
23
24
25
26
27
28
29
30
31
32
33
34
35
36
37
38
39
40
41
42
43
44
45
46
47
48
49
50
51
52
53
54
55
56
57
58
59
60